2020 IEEE/RSJ International Conference on Intelligent Robots and Systems (IROS)
October 25-29, 2020, Las Vegas, NV, USA (Virtual)

Robust Gait Design Insights from Studying a Compass Gait Biped with Foot Slipping

Tan Chen and Bill Goodwine[1]

Abstract— **Most current bipedal robots were modeled with an assumption that there is no slip between the stance foot and ground. This paper relaxes that assumption and undertakes a comprehensive study of a compass gait biped with foot slipping. It is found that slips are most likely to happen near impact for a broad range of gaits. Among these gaits, ones with a backward swing foot velocity relative to the ground just before touch down generally require less friction to maintain stable walking than ones with a forward relative foot velocity. Moreover, a larger percentage of gaits with the "swinging backward" foot can tolerate some slipping without falling than those with a swinging forward foot at touch down. Thus, a gait with the swing-backward foot just before touch down should be more robust in the sense of preventing slipping and falling. It is further shown that only one parameter in gait design determines the swing-backward feature, which can help design robust gaits. Models with varying physical parameters such as mass, leg length, and position of center of mass (CoM), are also studied to validate the generality of the results.**

I. Introduction

Currently the methods to control biped walking can be broadly classified as full actuation or underactuation. Humanoid robots such as Honda's Asimo [1] are actuated at all joints, and their walking is achieved by actuation of the hip, knee, and ankle joints. Underactuated robots have fewer actuators than the number of degrees of freedom, for example, they may be lack of ankle actuation [2] or hip actuation [3]. Many underactuated biped walking robots [2]–[7] are controlled with the hybrid zero dynamics (HZD) approach [8], which applies a Poincaré map to design stable, periodic walking gaits. All the aforementioned models assume that there is no foot slippage on the ground, and thus the stance foot can be treated as a stationary pivot point. To take the robot outside of human-made environment, however, foot slipping needs to be considered to make it able to walk on different terrains (such as a rainy, snowy or icy ground) and improve the robustness of biped robots [9], [10].

Boone and Hodgins [11] simulated a hopping two-leg robot on ground with different coefficients of friction by using reflex control, *i.e.*, the robot takes action immediately after it detects that a slip happens. They compared different strategies, and showed that to abandon the step by pulling the leg off the ground and re-positioning the robot is successful in recovering from slips on surfaces with very small coefficients of friction (as low as 0.07). Park and Kwon [12] proposed a reflex control method that elevates the hip (thus increasing the ground reaction force and friction force) and laterally drag the swing leg toward stance leg during swing phase (to keep the ZMP in a safety region). Their simulation on a 12-DoF fully actuated biped model showed that the robot can walk stably on the ground with the coefficient of friction as low as 0.3. Kajita et al. applied the preview control method on a fully actuated biped HRP-2 walking on a low friction floor [13], [14]. The biped was shown to be able to walk on a slippery floor with a friction coefficient of 0.14. However, the exact relationship among the slip- and stability-related indices proposed in their research was not fully resolved.

Recovery methods for when a foot slips require detection of slips. In simulation, slips are detected when the velocity of the stance foot is not zero or the horizontal acceleration of the stance foot is above a certain level, both of which may be difficult to detect in a real system. Kaneko et al. [15] defined a slip force, which is the difference between the actual reaction force and a reference reaction force. The slip force can be adopted as a slip observer in a physical robot. They also used the slip force to calculate the slip moment, which was considered to be the factor in posture rolling at slipping. Thus, they proposed a slip stabilizer to suppress posture rolling at slipping and experiments showed that the robot HRP-2 with the slip stabilizer can walk on the ground with a friction coefficient of 0.144.

Research focusing on underactuated bipeds has also recently started to consider foot slipping. The work in [16], [17] modeled slipping dynamics and provided a scheme to switch among multiple domains when a slip occurs. In [18], the authors experimentally demonstrated a foot slipping gait that can be stabilized on both a low-friction surface and a rough no-slip surface with the robot AMBER-3M.

This paper also studies foot slipping for underactuated bipeds, with a special focus on classification and characterization of all the feasible gaits that are obtained on a rough no-slip surface. It uses minimal coordinates to model a hybrid bipedal robot which allows for foot slipping, and further studies the causes of falling due to slipping, the relationships between slips and impact, gait feature and robustness (in the sense of preventing slipping and falling). The results are validated by using models with varying physical parameters. A simple robust gait design method is proposed and proven via simulation, considering a specific model, as opposed to proven mathematically.

*The partial support of the US National Science Foundation under grant IIS-1527393 is gratefully acknowledged.

[1]The authors are with the Department of Aerospace & Mechanical Engineering, University of Notre Dame, Notre Dame, IN 46556 USA, tchen8@nd.edu, bill@controls.ame.nd.edu.

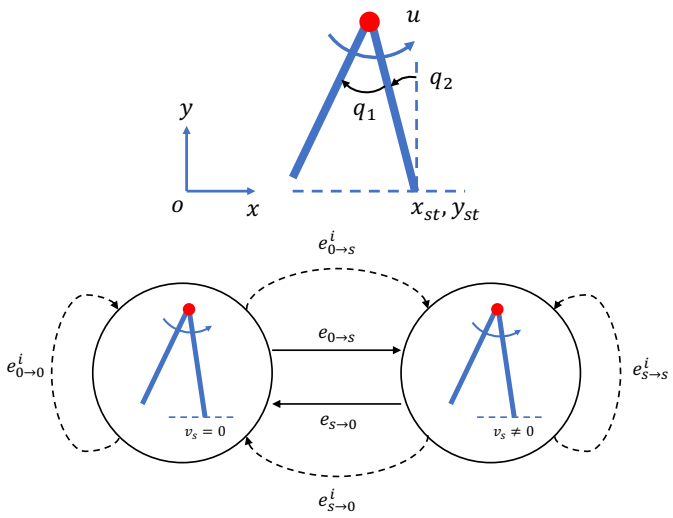

Fig. 1. Top: illustration of the hip-actuated compass gait biped in this paper. The legs are symmetric, with mass $m = 5$kg and length $l = 1$m for each. The location of the CoM of each leg is $lc = 0.8$m away from the foot, and the moment of inertia with respect to the CoM for each leg is $J = 0.6\text{kg}\cdot\text{m}^2$. Bottom: A general bipedal walking system consists of two modes: no slip (sticky) mode at the left side, and slip mode at the right side [18].

II. Foot Slipping for the Compass Gait Biped

The hip-actuated compass gait biped is illustrated in Fig. 1. Denote the hip and ankle joint angles as q_1 and q_2 respectively. The position of the stance foot is (x_{st}, y_{st}), and u is a torque applied at the hip. A general model consists of two modes: sticky mode[1] and slip mode. Thus, the system H [18], [19] can be expressed by

$$H = \{Q, X, f, Init, E, G, R\} \tag{1}$$

where

- $Q = \{0, S\}$, where 0 represents the sticky mode, and S represents the slip mode;
- $X = (q_1, q_2, x_{st}, y_{st}, \dot{q}_1, \dot{q}_2, \dot{x}_{st}, \dot{y}_{st}) \in \mathbb{R}^n$, represents the state space;
- $f : Q \times X \to \mathbb{R}^n$ assigns to each mode in Q an analytical vector field;
- $Init \subseteq Q \times X$ is the set of initial states;
- $E = \{e_{0\to s}, e_{s\to 0}, e^i_{0\to s}, e^i_{s\to 0}, e^i_{0\to 0}, e^i_{s\to s}\} \subseteq Q \times Q$ is the set of discrete transitions;
- $G = \{G(e) : e \in E\}$ is a set of guard conditions referring to the switching surfaces between different modes; and,
- $R = \{R(e) : e \in E\}$ is a set of reset maps.

A discrete transition event with a superscript i means that the transition happens at impact [18], which is also illustrated with a dashed line in Fig. 1. The other events occur during swing phases, such as $e_{0\to s}$ triggers when static friction force between the ground and stance foot cannot maintain sticky walking, and $e_{s\to 0}$ triggers when the stance foot velocity decreases from nonzero to zero.

[1]Sticky mode means that no slipping occurs at the mode, *i.e.*, the relative velocity between the surfaces of contact between the foot and the ground is zero.

A. Swing Phase in Each Mode

Compared with [16] that used excessive coordinates to model a biped with foot slipping, this paper adopted minimal coordinates to construct the model, *i.e.,* only 4 states $X_0 = \{q_1, q_2, \dot{q}_1, \dot{q}_2\}$ are needed to model the dynamics in the sticky mode, and 6 states $X_s = \{q_1, q_2, x_{st}, \dot{q}_1, \dot{q}_2, \dot{x}_{st}\}$ are used for the slip mode. The advantage of using minimal coordinates is that the dynamics at each mode are concise and the computation is relatively simple.

The dynamics for a swing phase at the sticky mode are

$$\begin{aligned}\dot{x} &= \begin{bmatrix} \dot{q} \\ D_0^{-1}(q)[-C_0(q,\dot{q})\dot{q} - G_0(q) + B_0(q)u] \end{bmatrix} \\ &= f_0(x) + g_0(x)u,\end{aligned} \tag{2}$$

where $q = [q_1, q_2]^T$ is the configuration, $x = [q_1, q_2, \dot{q}_1, \dot{q}_2]^T \in X_0$ is the state vector, u is the input, D_0 is the inertia matrix in sticky mode, C_0 is the Coriolis matrix, G_0 is the gravity vector, and B_0 is the input direction vector. The dynamics for a swing phase at the slip mode are

$$\begin{aligned}\dot{x} &= \begin{bmatrix} \dot{q} \\ D_s^{-1}(q)[-C_s(q,\dot{q})\dot{q} - G_s(q) + B_s(q)u + B_f(q)F_f] \end{bmatrix} \\ &= f_s(x,\dot{x}) + g_s(x)u,\end{aligned} \tag{3}$$

where $q = [q_1, q_2, x_{st}]^T$ is the configuration, $x = [q_1, q_2, x_{st}, \dot{q}_1, \dot{q}_2, \dot{x}_{st}]^T \in X_s$ is the state vector, u is the control input, F_f is the friction force, D_s, C_s and G_s are the corresponding matrices or vectors in slip mode, and B_f is the input direction vector for F_f.

The friction force F_f can be computed by $F_f = \mu_k F_n$, in which μ_k is the coefficient of kinetic friction, and F_n is the normal force computed by

$$\begin{aligned}F_n =& m\left(2g - (l+l_c)\cos q_2 \dot{q}_2^2 + (l-l_c)\cos(q_1 - q_2)(\dot{q}_1 - \dot{q}_2)^2\right) \\ & - m\left((l-l_c)\sin(q_1 - q_2) + (l+l_c)\sin q_2\right)\ddot{q}_2 \\ & + m(l-l_c)\sin(q_1 - q_2)\ddot{q}_1.\end{aligned}$$

Note that F_n is a function of $q, \dot{q}, \ddot{q}$, which is why f_s in Eq. (3) is a function of $x, \dot{x}$. Specifically, F_n is linear in $\ddot{q}$. This allows isolation of $\dot{x}$ onto one side, and thus, a standard numerical solver, such as Matlab's *ode45()*, can be used to compute a numerical solution to Eq. (3). Detailed expressions for the terms in Eq. (2) and (3) are in the Appendix.

B. Impact Map

Ignoring foot scuffing at mid-stance, as is typically done, touchdown occurs when the swing foot hits the ground, *i.e.*, the vertical position of the swing foot is 0 and the vertical velocity of the swing foot is negative. At touchdown, the model dynamics are

$$D_e\ddot{q}_e + C_e\dot{q}_e + G_e = \underbrace{B_e u}_{control} + \underbrace{J^T F}_{contact\ forces} + \underbrace{\delta F_{ext}}_{impact}, \tag{4}$$

where $q_e = [q_1, q_2, x_{st}, y_{st}]^T$ is an extended configuration state vector, $D_e \in \mathbb{R}^{4\times 4}$ is the extended inertia matrix, $C_e \in \mathbb{R}^{4\times 4}$ is the Coriolis matrix, $G_e \in \mathbb{R}^4$ is the gravity vector, J is a Jacobian matrix, $F = [F_f, F_n]^T$ are the contact forces

applied at the stance foot, and δF_{ext} are the generalized impact forces applied at the swing foot when it hits the ground. Integrating both sides of Eq. (4) within a very small amount of time δt, gives

$$D_e(q_e^+)\dot{q}_e^+ - D_e(q_e^-)\dot{q}_e^- = F_{ext}, \tag{5}$$

where q_e^+ and $\dot{q}_e^+$ are configuration and velocity states just after impact, q_e^- and $\dot{q}_e^-$ are configuration and velocity states just before impact, and $F_{ext} \in \mathbb{R}^4$ is a result of integrating the impulse force δF_{ext} over the impact duration δt. Refer to the Appendix for details about the extended inertia matrix D_e. Eq. (5) is also interpretable as an expression of conservation of momentum.

As slipping may occur just at the impact, it makes the configuration-based impact map in [8] not applicable. To obtain a general impact map, define the position of the swing foot $p_2 = (x_{td}, y_{td})^T = p_2(q_e)$, and the impulse at touch down as $F_2 = (F_2^t, F_2^n)^T$. Thus, the generalized impulse is

$$F_{ext} = [\frac{\partial}{\partial q_e} p_2(q_e)]^T \begin{bmatrix} F_2^t \\ F_2^n \end{bmatrix} \triangleq E_2(q_e^-)^T F_2, \tag{6}$$

where $E_2(q_e^-) \in \mathbb{R}^{2\times 4}$ is a Jacobian matrix, which projects from joint velocities to end-effector velocities, and $E_2(q_e^-)^T$ thus projects end-effector forces to joint torques.

Note that the configuration states at impact stay unchanged, and thus $q_e^+ = q_e^-$. Substituting Eq. (6) into (5), we have four equations and six unknowns, *i.e.,* $\dot{q}_e^+$ and F_2. The other two equations come from the constraints of configurations or contact forces.

1) When no slip happens at the impact, the swing foot sticks onto the ground with neither slip nor rebound,

$$E_2(q_e^-)\dot{q}_e^+ = 0_{2\times 1},$$

and so in matrix form,

$$\begin{bmatrix} D_e(q_e^+) & -E_2(q_e^-)^T \\ E_2(q_e^-) & 0_{2\times 2} \end{bmatrix} \begin{bmatrix} \dot{q}_e^+ \\ F_2 \end{bmatrix} = \begin{bmatrix} D_e(q_e^-)\dot{q}_e^- \\ 0_{2\times 1} \end{bmatrix}. \tag{7}$$

2) When slipping occurs at the impact and there is no rebound but slipping, *i.e.*,

$$\dot{y}_{td}^+ = \frac{\partial y_{td}}{\partial q_e}\dot{q}_e^+ = 0, \quad |F_2^t| = \mu_{kinetic}|F_2^n|,$$

and so in matrix form,

$$\begin{bmatrix} D_e(q_e^+) & -E_2(q_e^-)^T \\ \frac{\partial y_{td}}{\partial q_e} & 0_{1\times 2} \\ 0_{1\times 4} & [\pm 1, \mu] \end{bmatrix} \begin{bmatrix} \dot{q}_e^+ \\ F_2^t \\ F_2^n \end{bmatrix} = \begin{bmatrix} D_e(q_e^-)\dot{q}_e^- \\ 0 \\ 0 \end{bmatrix}. \tag{8}$$

III. Simulation Results and Analysis

A. Control of An Underactuated Biped Robot

An HZD-based controller [8] is adopted to control the hip-actuated biped robots studied in this paper. The idea is to actuate the hip joint q_1 in order to make it follow some desired trajectory $q_1'(q_2)$, which is a function of q_2 defined by a fourth-order Bézier polynomial. Because it completely specifies the motion, a trajectory $q_1'(q_2)$ is also called a gait.

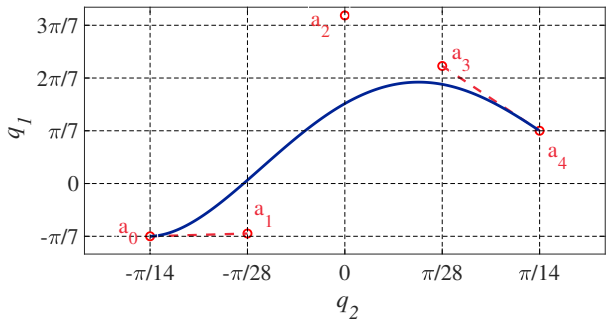

Fig. 2. A fourth-order Bézier curve defined by five control points, a_0 through a_4.

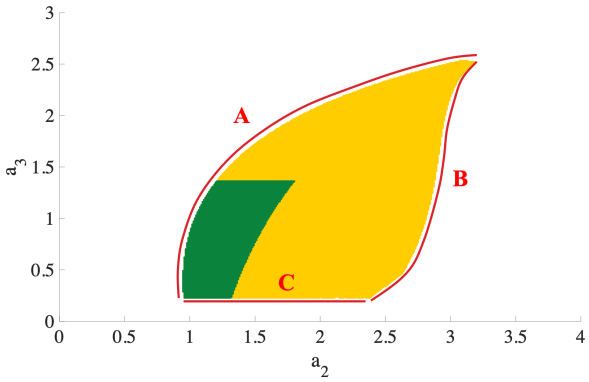

Fig. 3. The yellow and green region represents all the feasible gaits, and the green dots represent the gaits with a required coefficient of static friction μ_s that is less or equal to 1 to prevent slipping.

Some details about the Bézier polynomial will be important subsequently. Fig. 2 shows an example of a fourth-order Bézier curve. The curve is defined by a set of control points, a_0 through a_4. The first and last control points are the end points of the curve, and the second and second-to-last points help define the slopes at the two end points of the curve. Thus the gait is defined by

$$q_1'(q_2) = \sum_{k=0}^{4} a_k \frac{4!}{k!(4-k)!} \left(\frac{q_2 - q_2^+}{q_2^- - q_2^+}\right)^k \times \left(1 - \frac{q_2 - q_2^+}{q_2^- - q_2^+}\right)^{4-k}, \tag{9}$$

where q_2 is the ankle joint angle, q_1' is the desired hip joint angle, and q_2^- and q_2^+ are the ankle joint angles just before and after touch down, respectively, a_0 and a_4 are fixed by the end conditions of the gaits, and the jump condition at impact gives a relationship between a_1 and a_3. Therefore, only two parameters a_2 and a_3 are free to define the gait. Refer to [8, p. 138-144] for more details.

In this paper a fixed step length 0.445m is adopted to design the gaits and the gait curve starts at $(-\pi/14, -\pi/7)$ and ends at $(\pi/14, \pi/7)$, which requires $a_0 = -\pi/7$ and $a_4 = \pi/7$. Gaits on a 601×501 grid for $0 < a_2 < 6$ and $-2 < a_3 < 3$ are evaluated. Feasible gaits are defined such that:

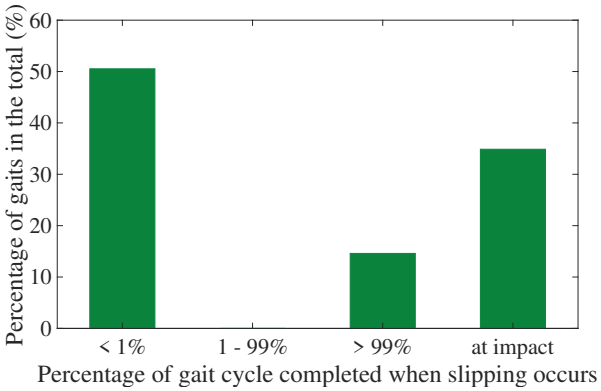

Fig. 4. When a slip happens for a feasible gait. $< 1\%$ represents that the most susceptible instant is at the first 1% cycle of a swing phase. $> 99\%$ represents that the instant is at the last 1% cycle of the swing phase, and $1-99\%$ indicates that the instant is in the middle of the swing phase. "at impact" indicates that the instant is just at the impact.

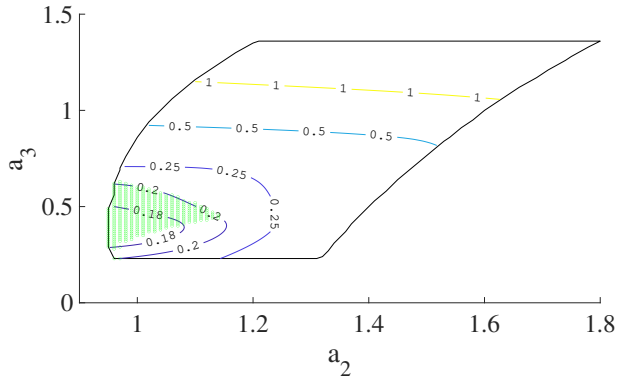

Fig. 5. The black boundary circles all the feasible gaits with a required $\mu_s \leq 1$ to prevent slipping. Each contour represents a level set of gaits with a specific CoT, which is numbered. Green dots represent all the gaits that fail on slippery ground because of falling backward. They generally have a small CoT ≤ 0.2. The other gaits fail on slippery ground because negative normal force is required.

1) there exists a real-value initial condition, 2) the normal force on the stance foot is always positive (unilateral contact force), 3) after impact the stance foot immediately lifts up without interaction with the ground, 4) the biped does not fall backward, 5) the joint velocities are within a reasonable range (under 100rad/s),[2] 6) the biped does not alternate the initially-designed step length. All the feasible gaits are shown in a colored region in Fig. 3. Outside boundary A, the biped can fall backward, because the unactuated ankle joint velocity becomes zero before the CoM of the biped passes the stance foot. Beyond the boundary B, negative normal force is required, which is not feasible. Below boundary C, the swing foot does not have negative vertical velocity when the foot reaches the ground, thus failing to hit the ground at the instant but keeping swinging.

B. Slip Friction and Falling Friction

Define the *slip friction* to be the minimum required coefficient of static friction that prevents slipping along the entire gait trajectory, including at impact. The slip frictions for all the feasible gaits in Fig. 3 range between 0.1 and several thousand. In order to make the contributions of this paper practically relevant, only the gaits with a slip friction less than or equal to 1 will be considered in the rest of this paper, which are shown in green in Fig. 3.

For all the feasible gaits in green, Fig. 4 shows at which stage in the gait slips occur. From Fig. 4, slips are most likely to happen at some instant in the neighborhood of impact, with 50% of the gaits where slipping happens just at the beginning of swing phase, 15% where slipping happens just before the impact, and the rest, 35%, where slipping happens just at impact. This intuitively makes sense, because our everyday experience is that a slip usually occurs just after touchdown in human locomotion.

On a surface with a low coefficient of friction slipping is likely to occur. Some gaits may be stable in the sense the robot does not fall and can continue to walk even if there is some foot slip during the gait cycle. Therefore, define the *falling friction* as the minimum required coefficient of static friction to maintain a stable walking without falling.

Throughout this paper we assume that the coefficient of static friction is 1.2 times the coefficient of kinetic friction. To obtain the falling friction for each feasible gait, the simulation starts with a friction coefficient that is slightly larger than the slip friction (0.002 greater), and repeats the simulation with the coefficient of friction decreased by 0.01 until the gait fails. The criteria used to determine a fall are that within 50 steps: 1) a negative normal force is required, 2) the biped falls backward, and 3) unreasonably large joint velocities are generated (greater than 100rad/s). It shows that on slippery ground the gaits fail either by falling backward (because the biped cannot move its CoM to pass over the stance foot), or by requiring negative normal force. Fig. 5 shows the distribution of these two types of gaits along with the Cost of Transport (CoT)[3]. For low CoT gaits, slipping can drain energy from the system, eventually leaving it without the energy necessary to take the next step.

A robust gait in the sense of preventing slipping or falling is a gait that requires relatively small slip friction and falling friction, and that can "tolerate" some slipping without falling. It is found that a very high percentage (over 99%) of gaits with a negative swing foot velocity relative to the ground (a "swing-backwards foot") just before touch down can tolerate some slipping without falling, as shown in Fig. 6. In contrast, about a half of gaits with swing-forward foot would fail once a slip occurs.

The left and right plots in Fig. 7 show the required slip friction and falling friction for all the feasible gaits, respectively. Note that color distribution on the two plots is similar, which suggests that a gait with small slip friction generally requires small falling friction.

[2]Actually all the obtained feasible gaits have relatively small joint speeds, much less than 100rad/s.

[3]Cost of Transport (CoT): smaller CoT means more energy efficiency.

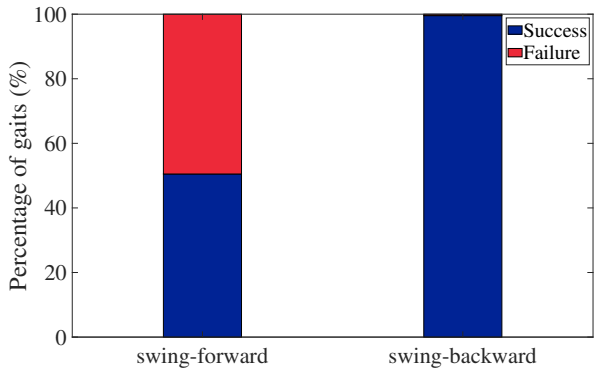

Fig. 6. Swing-forward (swing-backward) represents that the swing foot has a forward (backward) velocity just before touch down. Success (in blue) represents that a gait can tolerate some slipping without falling, and Failure (in red) represents that the gait fails once a slip occurs.

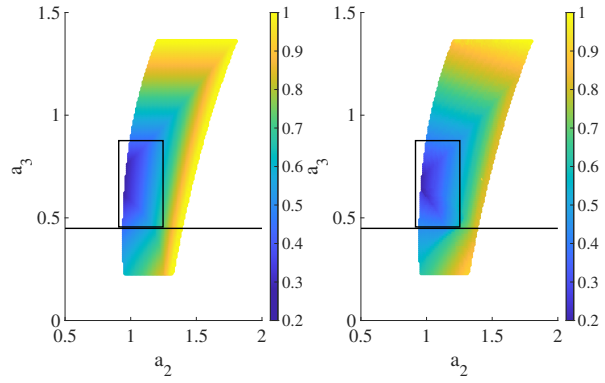

Fig. 7. Each dot is a feasible gait. Left: the color represents the magnitude of slip friction. Right: the color represents the magnitude of falling friction.

The feasible gaits can be split into two types, indicated in Fig. 7 by the black line. All the gaits with the swing-backward feature are above the line, while all the gaits with the swing-forward feature are below it. The gaits with relatively small slip and falling friction (that are in blue and outlined) are concentrated above the black line in both plots. Therefore, the optimally robust gaits have the swing-backward foot feature. The black line in Fig. 7 can be analytically computed. The x-directional velocity of the swing foot is

$$v_x = \dot{q}_2 l \cos q_2 + (\dot{q}_1 - \dot{q}_2) l \cos(q_1 - q_2).$$

Just before impact, the velocity is

$$v_x^- = \dot{q}_2^- l \cos q_2^- + (\dot{q}_1^- - \dot{q}_2^-) l \cos(q_1^- - q_2^-), \qquad (10)$$

where v_x^- is the x-directional velocity of the swing foot just before impact, q_1^- and q_2^- are hip and ankle joint angles just before impact, and $\dot{q}_1^-$ and $\dot{q}_2^-$ are hip and ankle joint velocities just before impact. Note that $q_1^- = 2q_2^-$ for a symmetric biped. Thus, it can be further simplified,

$$v_x^- = \dot{q}_1^- l \cos(q_1^- - q_2^-). \qquad (11)$$

TABLE I

BIPED MODELS WITH VARYING PARAMETERS.

Model Code	m (kg)	J (kg·m^2)	l (m)	l_c (m)
Model-0	5	0.6	1	0.8
Model-1a	1	0.12	1	0.8
Model-1b	10	1.2	1	0.8
Model-2a	5	0.14	0.5	0.4
Model-2b	5	1.3	1.5	1.2
Model-3a	5	0.5	1	0.7
Model-3b	5	0.55	1	0.75
Model-3c	5	0.65	1	0.85
Model-3d	5	0.7	1	0.9

Note that the term $\cos(q_1^- - q_2^-)$ is positive, and a positive (negative) $\dot{q}_1^-$ determines the swing-forward (swing-back) for a gait. The ankle joint angle q_2 is monotonically increasing in the HZD controller design, thus giving $\dot{q}_2^- > 0$. Therefore, to have a gait with the swing-back feature, it is required that $\dot{q}_1^-/\dot{q}_2^-$ should be negative. Recall in Fig. 2 that

$$\frac{\dot{q}_1^-}{\dot{q}_2^-} = \frac{a_4 - a_3}{\pi/28}, \qquad (12)$$

and thus $a_3 > a_4 = \pi/7$ gives a gait with the swing-backward feature, and $a_3 < a_4 = \pi/7$ gives a gait with the swing-forward feature. The value of a_3 is the line in Fig. 7 that differentiate the two types of gaits.

Even when a higher-order Bézier polynomial is adopted to design the gaits, the aforementioned result is applicable. The slope at the end point of the Bézier curve is defined by the last and second-to-last control points, as shown in Eq. (12). Thus, the second-to-last control point can always be used to design a robust gait with the swing-backward feature.

IV. EXTENSIONS TO MODELS WITH VARYING PARAMETERS

This section considers varying model parameters to verify that the results in Section III are not specific to the model parameters used for the nominal model. Table I lists different models for study. Model-0 is the nominal model. Model-1x represent models that vary masses relative to Model-0. Model-2x represent models that vary leg lengths. Model-3x represent models that vary positions of the CoM of the legs. These values are similar to the values taken for the compass gait biped model in [20].

Simulation shows that varying masses (Model-1x) or leg lengths (Model-2x) does not qualitatively affect the aforementioned results, *i.e.,* slips are most likely to happen near impact for all feasible gaits, and the gaits with the swing-backward feature are more robust in the sense of preventing slipping and falling. However, varying the CoM location of each leg (Model-3x) shows more complicated results, and thus five sets of models with different CoM positions are studied. See Model-0 and Model-3x in Table I.

For all the models with varying positions of CoM, it can still be observed that slips are most likely to happen at the instant in the neighborhood of impact. In Figs. 8-10, the x-axis, position of the leg CoM to the foot, represents the ratio

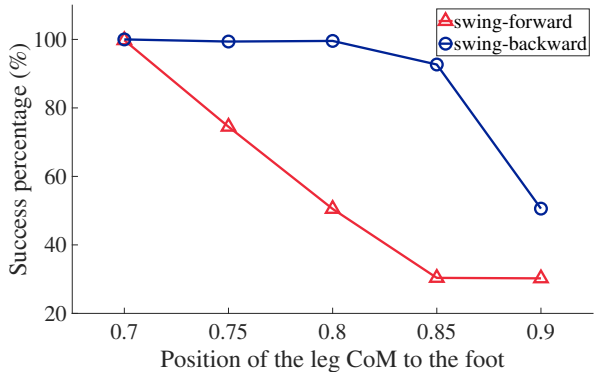

Fig. 8. Success percentage means the percentage of gaits that can tolerate some slipping with not falling. Blue dots represent the success percentages among the gaits with swing-backward feature, and red dots represent the success percentages among the gaits with swing-forward feature.

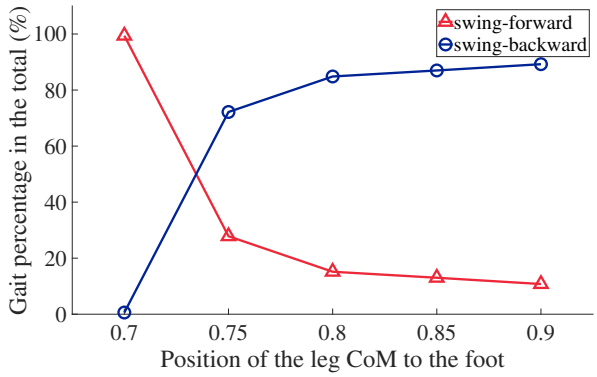

Fig. 9. Percentages of the two types of gaits in the feasible gait region, for models with varying positions of the leg CoM.

of distance between the foot and the leg CoM over the leg length. In an extreme case, if the CoM coincides with the foot, the value is 0.

Fig. 8 shows success percentages among the two types of gaits. The gaits with swing-backward feature have advantages over those with swing-forward feature almost through the whole range, and the advantage is the most significant at some point between 0.8 and 0.85.

When increasing the CoM location of each leg, the feasible region gets larger (which is not shown in this paper due to space limit). Along with that, the percentage of the gaits with swing-backward feature also gradually increases, as shown in Fig. 9. When the position is over 0.8, the increasing trend is no longer significant. Also note that when the CoM location of each leg is as low as 0.7, there are very few gaits with the swing-back feature.

Fig. 10 illustrates the slip and falling friction for the two types of gaits. Generally, the gaits that require the smallest slip and falling friction for different models have the swing-backward feature, which can be obtained by comparing the top two plots. The only exception is the Model-3a with the position of the CoM at 0.7: the gait with the smallest slip friction has the swing-forward feature. That is because there

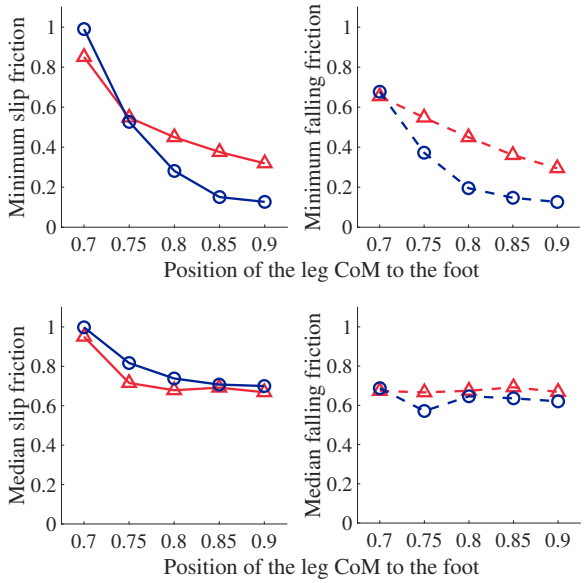

Fig. 10. Top-left: blue (red) dots represent the minimum slip friction among all the feasible gaits with the swing-backward (swing-forward) feature. Top-right: blue (red) dots represent the minimum falling friction among all the feasible gaits with the swing-backward (swing-forward) feature. Bottom-left: blue (red) dots represent the median slip friction among all the feasible gaits with the swing-backward (swing-forward) feature. Bottom-right: blue (red) dots represent the median falling friction among all the feasible gaits with the swing-backward (swing-forward) feature.

is nearly no gait with the swing-backward feature for the Model-3a. The bottom two plots compare the median slip and falling friction for the two types of gaits. The median slip friction for the gaits with the swing-forward feature is generally smaller than that for the the gaits with the swing-backward feature, partly due to the fact that the gaits with the swing-backward feature take a much larger percentage among all the feasible gaits as shown in Fig. 9. Even so, the median falling friction for the gaits with the swing-backward feature is generally smaller than that for the gaits with swing-forward feature. Therefore, the gaits with the swing-backward should be more robust in the sense of preventing slipping and falling.

Another observation from Fig. 10 is that the minimum and median slip/falling friction generally decrease as the biped has a higher CoM position of each leg. This suggests that increasing the CoM locations of the legs may help design a biped that is suitable for slippery ground. As the position of the CoM is over 0.8, the decreasing trend, however, is no longer significant. Also considering in Fig. 8 that the success rate for the gaits with the swing-back feature falls dramatically as the CoM position is over 0.85, an optimal biped design should be to select a position of the CoM at some point between 0.8 and 0.85.

V. Conclusions and Future Work

This paper studies the compass gait biped robot with foot slipping. It uses minimal coordinates to model the system, and presents the modeling of swing phases at sticky and slip modes and the derivation of a general impact map

in detail. It is found that slips are most likely to happen in the neighborhood of impact for models with varying parameters. The feasible gaits fail on slippery ground either by falling backward or by requiring negative contact force, which cannot be provided by the ground.

Two types of coefficients of friction are defined, slip friction and falling friction. Thus, a robust gait in the sense of preventing slipping and falling is a gait that requires small slip and falling friction to maintain stable walking, and that can tolerate some slipping without falling. By studying the models with varying parameters, the optimally robust gaits have a swing-backward feature. This result is consistent with that in [21], which shows that the swing leg retraction can improve biped walking stability. A CoM position at some point between 0.8 and 0.85 is an optimal design in increasing the robustness defined in this way. Furthermore, this paper also proves that the second-to-last control point in gait design using the Bézier curve determines the swing-backward feature, which is applicable to any order Bézier curve. Thus, it can guide the design of robust gaits in a simple way.

There are certain issues that require further work. This paper studies foot slipping with an assumption of Coulomb model of friction, which might not be applicable to some cases in reality. The friction model can be improved to make foot slipping results close to reality. Current gaits only consider a specific initial configuration, and a range of different configurations should be considered, which might affect foot slipping. Although many results initially obtained with simple models have generalized in biped locomotion, the results in this paper require validation on more complicated models such as a five-link and 3D biped in future.

VI. APPENDIX

Model parameters in Eq. (2) are [8]

$$D_0=\begin{bmatrix}D_{01} & D_{02}\\ D_{03} & D_{04}\end{bmatrix}\ C_0=\begin{bmatrix}C_{01} & C_{02}\\ C_{03} & C_{04}\end{bmatrix}\ G_0=\begin{bmatrix}G_{01}\\ G_{02}\end{bmatrix}\ B_0=\begin{bmatrix}1\\ 0\end{bmatrix}$$

where,

$$\begin{aligned}
D_{01} =& J+m(l-l_c)^2\\
D_{02} =& -J-m(l-l_c)(l-l_c-l\cos q_1)\\
D_{03} =& D_{02}\\
D_{04} =& 2J+ml_c^2+m(l^2+(l-l_c)^2-2l(l-l_c)\cos q_1)\\
C_{01} =& 0\\
C_{02} =& -ml(l-l_c)\sin q_1\dot{q}_2\\
C_{03} =& -ml(l-l_c)\sin q_1(\dot{q}_1-\dot{q}_2)\\
C_{04} =& ml(l-l_c)\sin q_1\dot{q}_1\\
G_{01} =& mg(l-l_c)\sin(q_1-q_2)\\
G_{02} =& -mg(l\sin q_2+l_c\sin q_2+(l-l_c)\sin(q_1-q_2)).
\end{aligned}$$

Model parameters in Eq. (3) are

$$D_s=\begin{bmatrix}D_{s1} & D_{s2} & D_{s3}\\ D_{s4} & D_{s5} & D_{s6}\\ D_{s7} & D_{s8} & D_{s9}\end{bmatrix}\ C_s=\begin{bmatrix}C_{s1} & C_{s2} & C_{s3}\\ C_{s4} & C_{s5} & C_{s6}\\ C_{s7} & C_{s8} & C_{s9}\end{bmatrix}$$
$$G_s=\begin{bmatrix}G_{s1}\\ G_{s2}\\ G_{s3}\end{bmatrix}\ B_s=\begin{bmatrix}1\\ 0\\ 0\end{bmatrix}\ B_f=\begin{bmatrix}0\\ 0\\ 1\end{bmatrix}$$

where,

$$\begin{aligned}
D_{s1} =& J+m(l-l_c)^2\\
D_{s2} =& -J-m(l-l_c)(l-l_c-l\cos q_1)\\
D_{s3} =& m(l-l_c)\cos(q_1-q_2)\\
D_{s4} =& D_{s2}\\
D_{s5} =& 2J+ml_c^2+m(l^2+(l-l_c)^2-2l(l-l_c)\cos q_1)\\
D_{s6} =& -m(l-l_c)\cos(q_1-q_2)+m(l+l_c)\cos q_2\\
D_{s7} =& D_{s3}\\
D_{s8} =& D_{s6}\\
D_{s9} =& 2m\\
C_{s1} =& 0\\
C_{s2} =& -ml(l-l_c)\sin q_1\dot{q}_2\\
C_{s3} =& 0\\
C_{s4} =& -ml(l-l_c)\sin q_1(\dot{q}_1-\dot{q}_2)\\
C_{s5} =& ml(l-l_c)\sin q_1\dot{q}_1\\
C_{s6} =& 0\\
C_{s7} =& -m(l-l_c)\sin(q_1-q_2)\dot{q}_1+2m(l-l_c)\sin(q_1-q_2)\dot{q}_2\\
C_{s8} =& -m(l-l_c)\sin(q_1-q_2)\dot{q}_2-m(l+l_c)\sin q_2\dot{q}_2\\
C_{s9} =& 0\\
G_{s1} =& mg(l-l_c)\sin(q_1-q_2)\\
G_{s2} =& -mg(l\sin q_2+l_c\sin q_2+(l-l_c)\sin(q_1-q_2))\\
G_{s3} =& 0.
\end{aligned}$$

Model parameters in Eq. (5) are [8]

$$D_e=\begin{bmatrix}D_{e1} & D_{e2} & D_{e3} & D_{e4}\\ D_{e5} & D_{e6} & D_{e7} & D_{e8}\\ D_{e9} & D_{e10} & D_{e11} & D_{e12}\\ D_{e13} & D_{e14} & D_{e15} & D_{e16}\end{bmatrix}$$

where,

$$\begin{aligned}
D_{e1} =& J+m(l-l_c)^2\\
D_{e2} =& -J-m(l-l_c)(l-l_c-l\cos q_1)\\
D_{e3} =& m(l-l_c)\cos(q_1-q_2)\\
D_{e4} =& m(l-l_c)\sin(q_1-q_2)\\
D_{e5} =& D_{e2}\\
D_{e6} =& 2J+ml_c^2+m(l^2+(l-l_c)^2-2l(l-l_c)\cos q_1)\\
D_{e7} =& m(l\cos q_2+l_c\cos q_2-(l-l_c)\cos(q_1-q_2))\\
D_{e8} =& -m(l\sin q_2+l_c\sin q_2+(l-l_c)\sin(q_1-q_2))\\
D_{e9} =& D_{e3}
\end{aligned}$$

$$
\begin{aligned}
D_{e10} &= D_{e7} \\
D_{e11} &= 2m \\
D_{e12} &= 0 \\
D_{e13} &= D_{e4} \\
D_{e14} &= D_{e8} \\
D_{e15} &= D_{e12} \\
D_{e16} &= 2m.
\end{aligned}
$$

Acknowledgments

The partial support of the US National Science Foundation under grant IIS-1527393 is gratefully acknowledged.

REFERENCES

[1] Y. Sakagami, R. Watanabe, C. Aoyama, S. Matsunaga, N. Higaki, and K. Fujimura, "The intelligent asimo: System overview and integration," in *Proceedings of the IEEE/RSJ International Conference on Intelligent Robots and Systems (IROS)*, vol. 3. IEEE, 2002, pp. 2478–2483.

[2] E. R. Westervelt, J. W. Grizzle, and D. E. Koditschek, "Hybrid zero dynamics of planar biped walkers," *IEEE transactions on automatic control*, vol. 48, no. 1, pp. 42–56, 2003.

[3] T. Chen, X. Ni, J. P. Schmiedeler, and B. Goodwine, "Using a nonlinear mechanical control coupling metric for biped robot control and design," in *Proceedings of the 22nd International Conference on Methods and Models in Automation and Robotics (MMAR)*. IEEE, 2017, pp. 903–908.

[4] C. Chevallereau, G. Abba, Y. Aoustin, F. Plestan, E. Westervelt, C. C. de Wit, and J. Grizzle, "Rabbit: A testbed for advanced control theory," *IEEE Control Systems Magazine*, vol. 23, no. 5, pp. 57–79, 2003.

[5] E. R. Westervelt, G. Buche, and J. W. Grizzle, "Experimental validation of a framework for the design of controllers that induce stable walking in planar bipeds," *The International Journal of Robotics Research*, vol. 23, no. 6, pp. 559–582, 2004.

[6] T. Yang, E. Westervelt, A. Serrani, and J. P. Schmiedeler, "A framework for the control of stable aperiodic walking in underactuated planar bipeds," *Autonomous Robots*, vol. 27, no. 3, p. 277, 2009.

[7] B. G. Buss, A. Ramezani, K. A. Hamed, B. A. Griffin, K. S. Galloway, and J. W. Grizzle, "Preliminary walking experiments with underactuated 3d bipedal robot marlo," in *2014 IEEE/RSJ International Conference on Intelligent Robots and Systems*. IEEE, 2014, pp. 2529–2536.

[8] E. R. Westervelt, J. W. Grizzle, C. Chevallereau, J. H. Choi, and B. Morris, *Feedback control of dynamic bipedal robot locomotion*. CRC press, 2007, vol. 28.

[9] "Marlo walks in the snow, uphill!" [Online]. Available: https://www.youtube.com/watch?v=Gusf8-bWchg

[10] "Cassie blue's first time to play in the snow." [Online]. Available: https://www.youtube.com/watch?v=GSbYHArd5o8

[11] G. N. Boone and J. K. Hodgins, "Slipping and tripping reflexes for bipedal robots," *Autonomous robots*, vol. 4, no. 3, pp. 259–271, 1997.

[12] J. H. Park and O. Kwon, "Reflex control of biped robot locomotion on a slippery surface," in *Proceedings 2001 ICRA. IEEE International Conference on Robotics and Automation (Cat. No. 01CH37164)*, vol. 4. IEEE, 2001, pp. 4134–4139.

[13] S. Kajita, F. Kanehiro, K. Kaneko, K. Fujiwara, K. Harada, K. Yokoi, and H. Hirukawa, "Biped walking pattern generation by using preview control of zero-moment point," in *Proceedings of the IEEE International Conference on Robotics and Automation (ICRA)*, vol. 3, 2003, pp. 1620–1626.

[14] S. Kajita, K. Kaneko, K. Harada, F. Kanehiro, K. Fujiwara, and H. Hirukawa, "Biped walking on a low friction floor," in *2004 IEEE/RSJ International Conference on Intelligent Robots and Systems (IROS)*, vol. 4. IEEE, 2004, pp. 3546–3552.

[15] K. Kaneko, F. Kanehiro, S. Kajita, M. Morisawa, K. Fujiwara, K. Harada, and H. Hirukawa, "Slip observer for walking on a low friction floor," in *2005 IEEE/RSJ International Conference on Intelligent Robots and Systems*. IEEE, 2005, pp. 634–640.

[16] B. Gamus and Y. Or, "Dynamic bipedal walking under stick-slip transitions," *SIAM Journal on Applied Dynamical Systems*, vol. 14, no. 2, pp. 609–642, 2015.

[17] K. Chen, M. Trkov, J. Yi, Y. Zhang, T. Liu, and D. Song, "A robotic bipedal model for human walking with slips," in *2015 IEEE International Conference on Robotics and Automation (ICRA)*. IEEE, 2015, pp. 6301–6306.

[18] W.-L. Ma, Y. Or, and A. D. Ames, "Dynamic walking on slippery surfaces: Demonstrating stable bipedal gaits with planned ground slippage," in *2019 International Conference on Robotics and Automation (ICRA)*. IEEE, 2019, pp. 3705–3711.

[19] H. Lin, P. J. Antsaklis, *et al.*, "Hybrid dynamical systems: An introduction to control and verification," *Foundations and Trends® in Systems and Control*, vol. 1, no. 1, pp. 1–172, 2014.

[20] T. Chen, J. P. Schmiedeler, and B. Goodwine, "Robustness and efficiency insights from a mechanical coupling metric for ankle-actuated biped robots," *Autonomous Robots*, vol. 44, no. 2, pp. 281–295, 2020.

[21] M. Wisse, C. G. Atkeson, and D. K. Kloimwieder, "Swing leg retraction helps biped walking stability," in *5th IEEE-RAS International Conference on Humanoid Robots, 2005.* IEEE, 2005, pp. 295–300.